

# Structural and optical characterization of ZnO and AZO thin films: the influence of post-annealing

Laya Dejam<sup>1</sup> · S. Mohammad Elahi<sup>1</sup> · Heydar Honarvar Nazari<sup>2</sup> · Hossein Elahi<sup>3</sup> · Shahram Solaymani<sup>4</sup> · Atefeh Ghaderi<sup>4</sup>

Received: 14 July 2015 / Accepted: 27 September 2015 / Published online: 5 October 2015  
© Springer Science+Business Media New York 2015

**Abstract** In the present study, ZnO and Al:ZnO (AZO) thin films were prepared by reactive RF sputtering on quartz substrates at a constant oxygen partial pressure and a typical sputtering power. Films were annealed at different temperatures in argon ambient in the oven to study their various structural and optical properties. It was understood that introducing Al into ZnO structure would affect the ZnO crystalline structure noticeably. It was observed that annealing had great influence on various properties of thin films while ZnO film showed low crystallinity, Al doping into ZnO structure pronounced significant improvement in both crystallinity and particle sizes. It was found that crystal structures, average crystalline sizes, and topology of all thin films were modified enormously by post-annealing. It was shown that films transparency fluctuated by annealing, in which the transparency of AZO thin film annealed at 500 °C was much greater than others. Annealing led to decrease optical band gap of all annealed films from 3.31 to 3.26 eV for ZnO and 4 to 3.4 eV for AZO films. Photoluminescence manifested that blue emission in as-deposited film led to two different blue and violet emissions in all AZO and ZnO films. It was

identified that the emission intensity of AZO film annealed at 500 °C was 12 times more than other ZnO and AZO films.

## 1 Introduction

Zinc oxide nanomaterial has been studied vastly by many researchers owing to the various and versatile features, including being a wide and direct band gap material (3.37 eV) [1], having high exciton binding energy [2], being a low-loss plasmonic material [3], and high electron mobility [2]. Therefore, it has been used for myriad applications in solar cell, both thin films [4] and dye-synthesized solar cell (DSSC) [2], light emitting diodes (LED) [5], transparent conductive oxide (TCO) [6], gas sensors [7], and as a mid-layer in thin film solar cells [8]. Amongst different metal oxides, probably zinc oxide has the most different nano-shapes comprise nanowire [9], nanorod [10], hollow nanospheres [11], colloidal nanoparticles [12], and nanotube [13] which they are still under intensive researches. A host of different groups have developed this metal oxide semiconductor (MOS) thin film by variety of methods such as DC magnetron sputtering [14], RF sputtering [15], metal organic chemical vapor deposition (MOCVD) [16], thermal-evaporation [17]. Amongst all these techniques, RF sputtering has created a great opportunity to deposit the film by easily controlling the rate of deposition, low produced temperature, and high crystallinity seeing that low rate of deposition [18]. Many researches have been devoted to study zinc oxide and doping the material with variety of elements, such as Ga, N<sub>2</sub>, and..., to improve their properties for various applications. However, Al doping showed that it could cause both widening band gap and improving electrical properties of ZnO by

✉ S. Mohammad Elahi  
smohammad\_elahi@srbiau.ac.ir

<sup>1</sup> Department of Physics, Science and Research Branch, Islamic Azad University, Tehran, Iran

<sup>2</sup> Faculty of Environment and Energy, Science and Research Branch, Islamic Azad University, Tehran, Iran

<sup>3</sup> Department of Mechanical Engineering, Arak University of Technology, Arak, Iran

<sup>4</sup> Young Researchers and Elite Club, Kermanshah Branch, Islamic Azad University, Kermanshah, Iran

increasing carrier concentration to be utilized as a TCO [19]. Abundance of Al, Zn, and O<sub>2</sub> compared to indium shortage has intrigued researchers to focus on AZO rather than In:SnO<sub>2</sub> (ITO) which had stability issues [20]. Photoluminescence properties of ZnO modified enormously by introducing variety of defects to ZnO thin films such as annealing in Ar, N<sub>2</sub>, O<sub>2</sub>, and H<sub>2</sub> atmospheres affecting various properties of ZnO films [21–24] depending on the sort of defects introduced to thin films. However, annealing with argon has not been extensively studied so far.

The major aim of the current study was to verify structural, topology, optical, and structural properties of both ZnO and AZO thin films. Moreover, PL manifested annealing and Al doping effects on structural defects of ZnO. It was clarified that annealing in Ar atmosphere and Al doping cause to enhance extremely both blue and violet emissions.

## 2 Experiments

ZnO and Al:ZnO (AZO) thin films were prepared on quartz substrates by Radio-frequency magnetron sputtering. Sputtering gas was Ar and O<sub>2</sub> with the  $\frac{O_2}{O_2+Ar}$  ratio of 30 % and remained constant during operation by employing two rotary and turbo pumps. Power of sputtering was 125 W for deposition of both ZnO and AZO films. Base pressure was  $2 \times 10^{-4}$  mbar and initial vacuum for sputtering was  $7.8 \times 10^{-3}$  mbar. To remove any possible impurity, substrates were cleaned by distilled water. Then, they were

placed in ethanol and acetone in ultrasonic cleaner for 20 min. Finally, they were washed by distilled water and dried in a clean room. Target was sputtered for 30 min to remove any possible oxide. Al–Zn metal target was disk with diameter of 77 mm and thickness of 3 mm of 90 % Zn + 10 % Al both in purity of 99.99 were melted at 600 °C to reach Al–Zn target. Thickness of deposited films was  $230 \pm 5$  nm as measured by a quartz crystal monitor during deposition. DEKTAK 3 profilometer was employed for measuring the thickness after deposition. Films were deposited on quartz substrates at room temperature. After deposition, temperature in chamber was measured 27 °C. Annealing was carried out in a furnace by argon flux at three different temperatures of 400, 500, and 600 °C for 1 h with the rate of 10 °C/min to consider post-annealing effects on different properties of thin films. They cooled down gradually to ambient temperature. To measure weight and atomic ratios elements of AZO films and the target, scanning electron microscopy (SEM), VEGA-TESCAN LMU in EDX mode, was employed and the results are shown in Fig. 1. To identify crystallite structure of thin films, STOE-XRD diffractometer using Cu-K<sub>α</sub> line ( $\lambda = 0.15406$  nm) was used. Optical measurements were performed by Varian Cary-500 spectrophotometer in the range of 200–2500 nm (Varian Inc., CA, USA). Topology and RMS roughness of thin films were determined by Veeco-Autoprobe in contact mode. Photoluminescence was utilized to point out luminescence characteristics of thin films by Cary Eclipse spectrometer equipped with a xenon lamp with 320 nm excite wavelength. All measurements were made at room temperature.

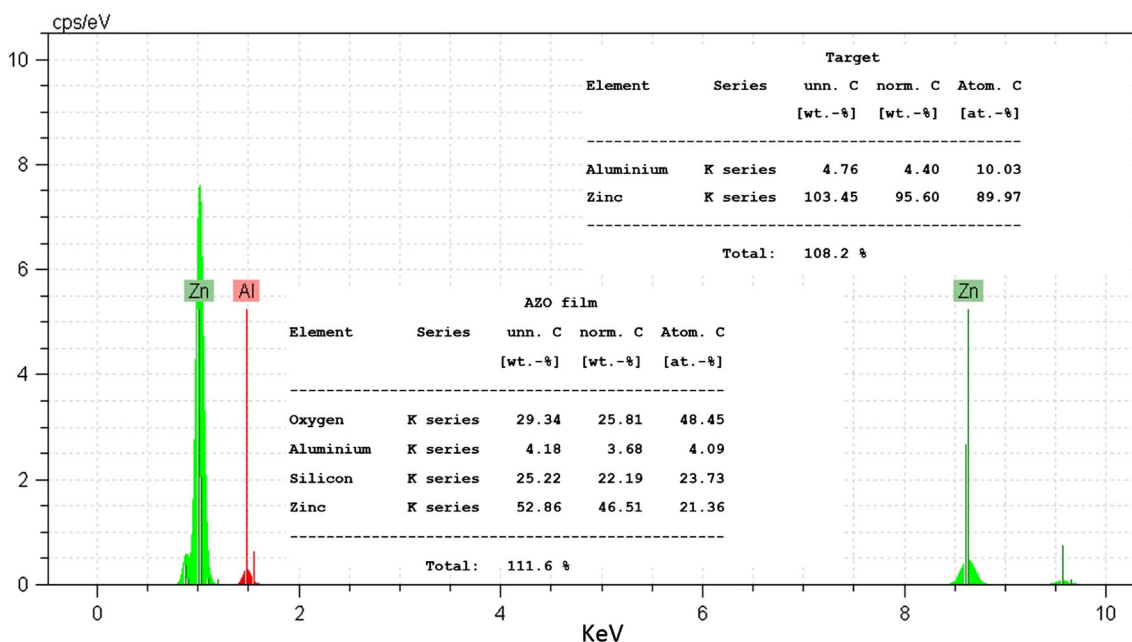


**Fig. 1** Edx spectrum of Al–Zn target. Inset: percent elements in target and AZO thin film

### 3 Results and discussion

#### 3.1 Structural properties of ZnO and AZO thin films

Figure 2 illustrates XRD analysis of ZnO thin films. All ZnO films characterizations indicated the hexagonal wurtzite structure showing (002) c-axis preferred orientation. As-deposited ZnO and annealed film at 400 and 600 °C experienced one peak which occurred at 34.072, 34.8898, and 34.593°, respectively. Unlikely, annealed film at 500 °C signified four different crystal orientations at 31.85, 34.46, 36.358, and 56.75° correspond to (100), (002), (101), and (110) directions, respectively. It could be understood that all ZnO films, both as-deposited and annealed at different temperatures, showed high crystallinity with hexagonal crystal structure as expected. The peaks intensity and the peak position at (002) changed by varying annealing temperatures. Changing the shift of

peaks towards the higher angle would be due to the relaxation of the strain [25]. It could be explained that, annealing at higher temperatures led to improvement of the crystallinity. Improvement of crystalline quality by increasing annealing temperature could be related to mobility enhancement of particles [26]. It seems that annealing at 500 °C, is a critical point in which the evaporation of trapped oxygen atoms in vacancies led to stoichiometry modification which resulted in distortion of crystallinity [20].

To calculate average crystalline sizes of deposited films, Debye–Scherrer equation was used as following [27] and the results are shown in Table 1:

$$\tau = 0.9\lambda/\beta \cos \theta \tag{1}$$

where  $\lambda$  stands for wavelength in nm,  $\beta$  is FWHM at half-maximum, and  $\theta$  is the angle at which the most intense peak occurred (called the Bragg angle). The results are shown in Table 1. As it is clear from Table 1,

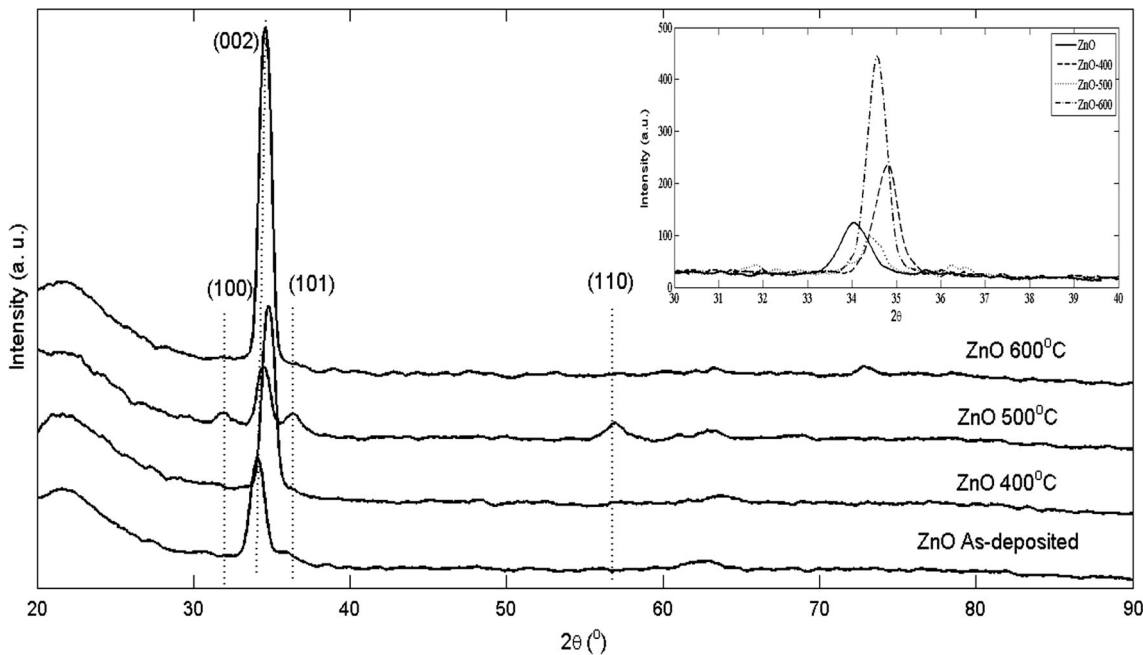


Fig. 2 XRD patterns of ZnO thin films annealed at different temperatures

Table 1 XRD analysis details of ZnO films

Annealing temperatures (°C)	Angle 2θ (°)	Lattice constant (Å)	FWHM (deg)	Crystalline size (nm)	RMS roughness (nm)	$\alpha_c \times 10^{-6} \text{ k}^{-1}$
As-deposited	34.072	5.26	0.5760	25.17	6.15	–
400	34.889	5.14	0.5280	27.55	8.84	0.616
500	34.46	5.20	0.3936	36.87	7.49	0.103
600	34.593	5.18	0.2230	37.25	9.42	0.266

the crystalline size and the angle at 34.593 which the peak (002) is located, is increased by increasing the annealing temperature. So it could be possible to state that the post annealing led to the evaporation of trapped oxygen atoms in vacancies which is resulted to increase of crystalline size. Preferential crystal orientation of (002) was more likely to grow at lower temperatures which could signify that their surface free energy but for annealed ZnO film at 500 °C, due to the increment of free surface energy, other crystal orientation were also noticed [28]. However, by increasing annealing temperature to 600 °C, at first different defects in the film were eliminated and a highly crystalline film at crystal orientation of (002) was grown. Therefore, it causes an increase of thermal expansion coefficient of annealed ZnO film at 600 °C direction of c axis ( $\alpha_c$ ). Expansion coefficient for all studied ZnO thin films are listed in Table 1. The lattice parameters of semiconductors pertained to various factors, such as temperature, and it would be determined by expansion coefficient relation. Expansion coefficient of in-plane and out-of-plane could be calculated by  $\alpha_a = \Delta a/a$  and  $\alpha_c = \Delta c/c$ , respectively [29]. It could be seen that  $\alpha_c$  for ZnO annealed thin film at 500 °C was the lowest amongst all ZnO thin films. This phenomenon would be related to the fact that by increment of annealing temperature to 500 °C, expansion was experienced in both a axis and c axis, in-plane and out-of-plane respectively, therefore as it is shown in Fig. 1 different crystal orientations were obtained. On the other hand,  $\alpha_c$  increased by increment of annealing temperature to 600 °C annealed and it is twice as high as those films annealed at 500 °C.

The results of XRD analysis of AZO thin films is indicated in Fig. 3. It could be observed that there was no noticeable peak in as-deposited AZO which illustrated that the film was amorphous in nature. By annealing AZO thin film at 400 °C, two different peaks occurred at 31.35 and 36.69 degrees correspond to (100) and (101), respectively. Further annealing at 500 °C showed that instead of the preferential orientation in (002) direction at 33.87 a small peak occurs at 36.89 which shows the (101) crystal orientation. Unlikely, by increasing annealing temperature to 600 °C, it led not only to lower crystallinity, but it also resulted in two peaks which happened at 31.44 and 57.50 correspond to (100) and (110), respectively. Besides, the second peak intensity of AZO film annealed at 600 °C was more than other one in the film. Considering the ratio of oxygen to argon during deposition of AZO, which was 3:7, and amount of aluminum in the target, there was no enough circumstance to allow the film to obtain any crystalline preferential orientation. However, by post annealing, trapped oxygen atoms between grain boundaries evaporated and since AZO grains surfaces energy increased; they could grow a small crystalline orientation with low intensity. When AZO film annealed at 500 °C, it resulted in c-axis orientation growth due to improve the stoichiometry. On the contrary, by annealing to 600 °C, lattice mismatched happened following from stoichiometry disturbance. Lower intensity of AZO annealed at 600 °C compared with AZO annealed at 500 °C could be related to the duration of annealing.

In AZO films annealed at 500 °C, particle sizes increased. This result could be also observed in XRD analysis which indicated that the film crystallinity of AZO

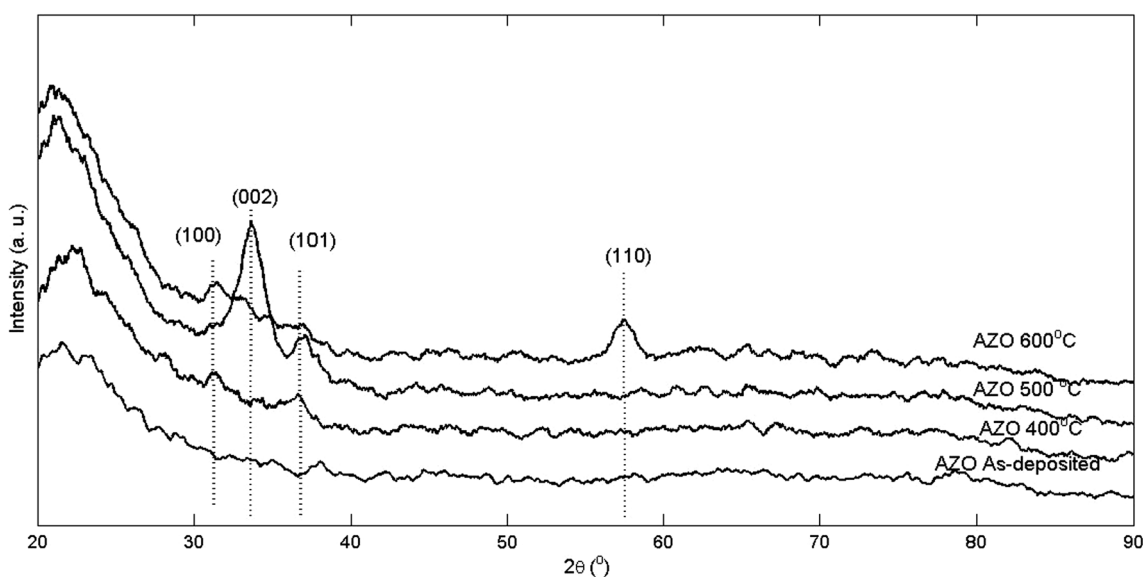


**Fig. 3** XRD patterns of AZO thin films annealed at different temperatures

films annealed at 500 °C was the greatest amongst all AZO films. However, by increasing annealing temperature to 600 °C, particle sizes increased. The reason would be the increment of surface diffusion owing to higher annealing temperature [30]. Unlikely, its crystalline quality decreased since by increasing annealing temperature, agglomeration increased, which resulted in increasing particle sizes, yet annealing duration which would be needed to increase crystalline intensity was not sufficient due to argon inert nature in comparison with reactive gases including oxygen [18]. According to Table 2, the grain size is increased by increasing annealing temperatures. It was highlighted by Lin et al. [20] that annealing could lead to disturbance of grain boundaries resulting in sticking grains to one another. By increasing the annealing temperature the grain size of both ZnO and AZO thin films were increased. This modification was also observed in AFM topology. Table 2 reports the XRD analysis of AZO films.

Figure 4 indicates surface topology of ZnO and AZO films carried out by AFM analysis. It could be observed that ZnO particles were located close to one another in as-deposited film and with a circle-shape. However by increment of annealing temperature to 500 °C, the shapes of particles gradually turned to oval and then to circle at higher temperatures about 600 °C. These behaviors could be related to  $\alpha_c$  which decreased by annealing to 500 °C and increased when ZnO film was annealed to 600 °C as obtained by XRD analysis. The change of particle shapes could be related to the variation of  $\alpha_c$  by annealing from 500 to 600 °C (Table 1).

As it is evident in AFM images (Fig. 4.) of the as-deposited and annealed AZO films, they were not like ZnO annealed films at the same temperatures. We can relate this issue to Al atoms in ZnO thin films and doping played a great role in this matter. RMS roughness of ZnO films was in the range 6.15–9.42 nm. By annealing of ZnO thin films, RMS roughness increased generally. On the other hand, RMS roughness of AZO thin films showed the films roughness in the range of 2.57–4.06 nm. Unlike the ZnO films, the RMS roughness of AZO film did not change when annealed in argon gas in the temperatures ranges

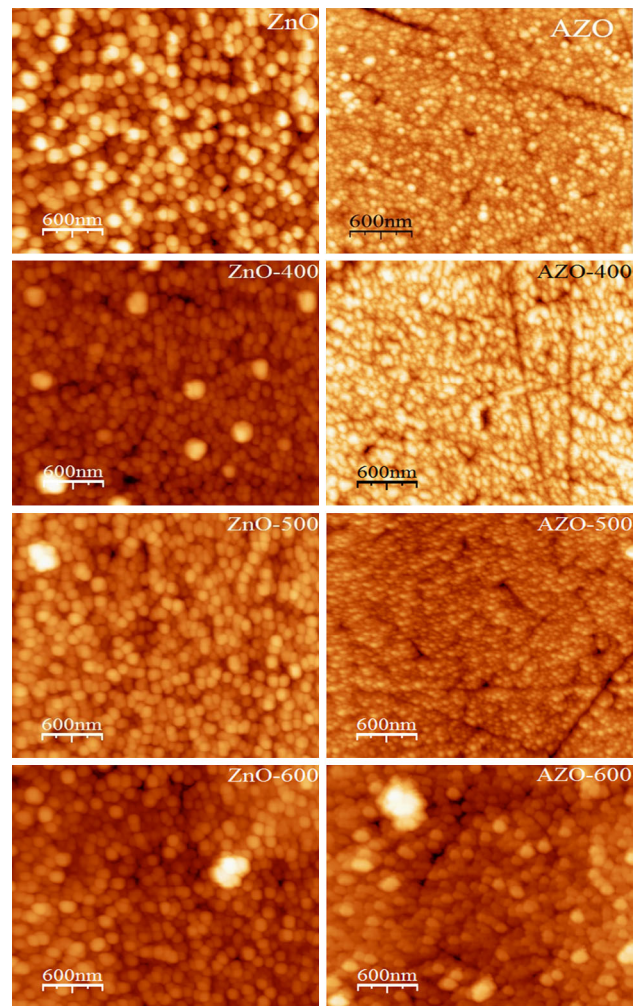


**Fig. 4** AFM images of ZnO and AZO thin films annealed at different temperatures

from 400 to 600 °C. RMS roughness of AZO films was less than ZnO films. Besides, the lowest RMS roughness in AZO films was attributed to the film annealed at 500 °C. As being discussed previously, the film crystallinity improved noticeably by annealing at 500 °C compared with others.

**Table 2** XRD analysis details of AZO films

Annealing temperatures °C	Angle 2θ (°)	Lattice constant (Å)	FWHM (deg)	Crystalline size (nm)	RMS roughness (nm)
As-deposited		–	–	–	3.50
400	31.35	A = 3.29	0.4076	13.7	4.06
	36.69	C = 4.9	1.065		
500	33.87	A = 3.18	0.2585	18	2.57
	36.89	C = 5.29	0.8209		
600	31.44	A = 3.28	0.020	39	3.87
	57.50	–	0.405		

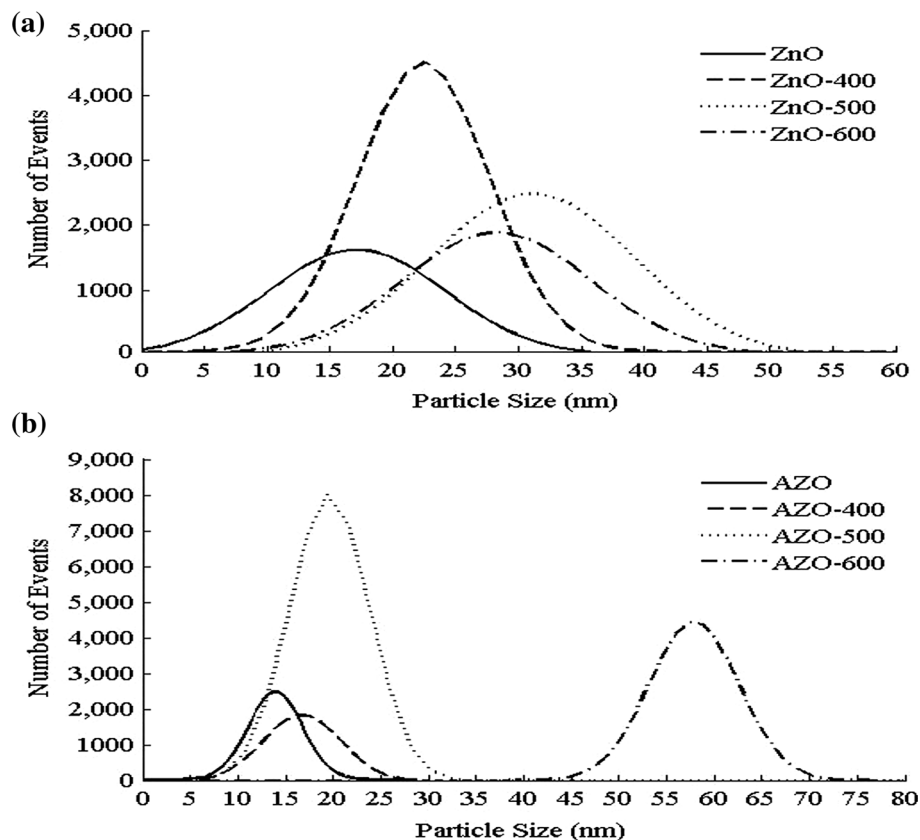
Figures 5 and 6 indicate the distribution of nano-particles for ZnO and AZO films. In ZnO thin films, as annealing temperature increased, particle sizes increased from 20 to 30 nm. It could be stemmed that annealing led to the increase of particle sizes owing to increment of surface diffusion. Furthermore, by increment of annealing temperature, distribution of nano-particles in the films did not modify significantly. In AZO films, by annealing particle sizes increased to 58 nm that it could be inferred that the modification was attributed to crystalline structures of AZO films and the fact that by improvement of thin films crystallinity, particle sizes increased [31]. By comparing the AFM images of ZnO and AZO, one noticed that the size of nano-particles in both as-deposited films are different, as illustrated in Figs. 5 and 6. However, it could be observed that annealing, at the same condition led to increase particle sizes in ZnO films, while particle sizes decreased in majority of AZO films. Particle sizes of ZnO film annealed at 500 °C were two times bigger than AZO annealed at the same temperature (Table 1, 2). As-deposited AZO was amorphous and annealing resulted in improvement of AZO films crystallinity (Fig. 3). On the contrary, annealing of ZnO films led to improvement of surface diffusion and sticking of nano-particles to one another.

### 3.2 Optical properties of ZnO and AZO thin films

Figures 7 and 8 present transmittance of ZnO and AZO films versus wavelength. All as-deposited and annealed ZnO films were highly transparent and the annealing process resulted in improvement of transparency. Although 80 % transparency of ZnO film followed after annealing at 500 °C, annealing of ZnO at 600 °C led to slightly decreased in transparency. Compared with transparency of AZO film annealed at 400 °C, all ZnO films were lower. Interestingly, annealing AZO films at higher temperatures resulted in ~90 % transparency. Modification of transparency in thin films could pertain to crystalline structure and nano-particle sizes. It could be inferred that by increment of annealing temperature, crystalline structure improved, so films transparency is increased. As being reported by other researchers [32], the transparency of films with amorphous structures was smaller than films with greater crystallinity.

Absorption coefficients of ZnO and AZO films, were calculated by  $T = A \exp(-\alpha d)$ , where  $T$  is the transmittance of thin film,  $A$  is a constant, and  $d$  is the film thickness, the results are shown in Fig. 7. It could be understood that by annealing and also, increment of annealing temperature, a red shift was experienced in absorption edge. By annealing,

**Fig. 5** Distribution of particle size of **a** ZnO thin films **b** AZO thin films annealed at different temperatures



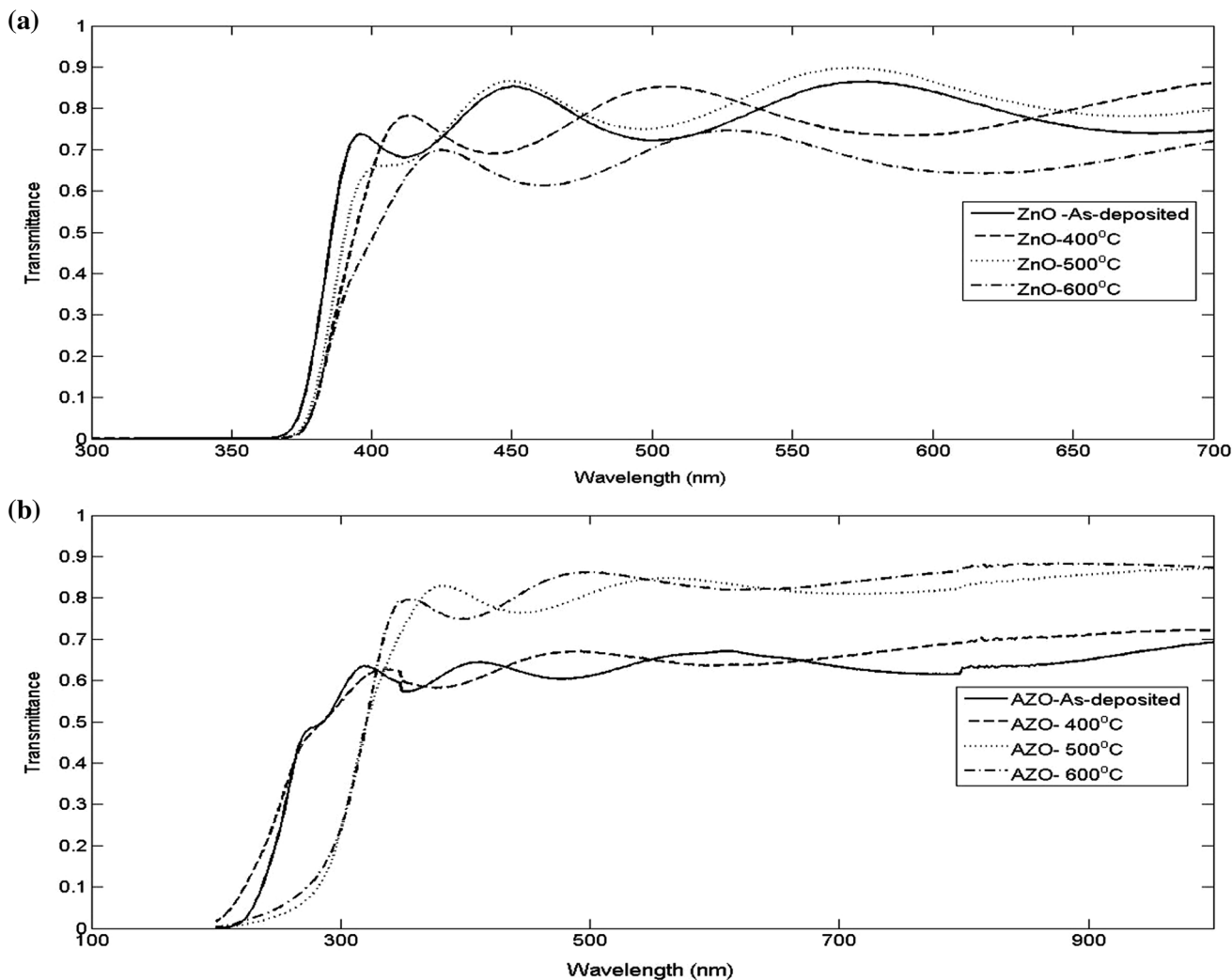


**Fig. 6** Transmission spectra of **a** ZnO thin films and **b** AZO annealed at different temperatures

a very slight shift in absorption edge was obtained despite the fact that for AZO films annealed at 500 and 600 °C, the red shift was more pronounced than AZO annealed at 400 °C (Table 2).

In absorption spectra of ZnO films, free exciton peaks could be observed which were indicated by arrow. It was illustrated that by variation of annealing temperature, exciton peaks were modified. The peak could be assumed to be free exciton in absorption spectra due to the fact that no the same behavior was observed in AZO films (Fig. 7). Because Al impurities release free electrons and holes that can screen the Coulomb interaction in the exciton and thereby strongly reduce the binding forces [33]. Therefore, excitonic effects were not observed in doped ZnO, since they contain a very high density of free carriers.

Tauc method was used to measure the band gap of thin films as follows [34]:

$$(\alpha h\nu)^m = A(h\nu - E_g) \tag{2}$$

where  $h$  is Planck constant,  $A$  is a constant,  $\nu$  is frequency of light and  $E_g$  is the band gap. It was reported that the value of  $m$  depends on various factors which should be determined before being employed in Tauc relation. It could be 1/2, 2, 3/2, or 3 depends on being indirect band gap, direct band gap, allowed or forbidden, respectively [28]. Figure 8 illustrates measured optical band gap by plotting  $(\alpha h\nu)^m$  versus  $h\nu$  for ZnO and AZO films. Optical energy band gaps of ZnO and AZO thin films were calculated and the results are indicated in Table 3. By annealing ZnO films, optical band gap decreased. The results were comparable with the results of particle sizes in AFM analysis; which showed the particle sizes increased by increment of annealing temperature. On the contrary, band gap decreased by increasing annealing temperature

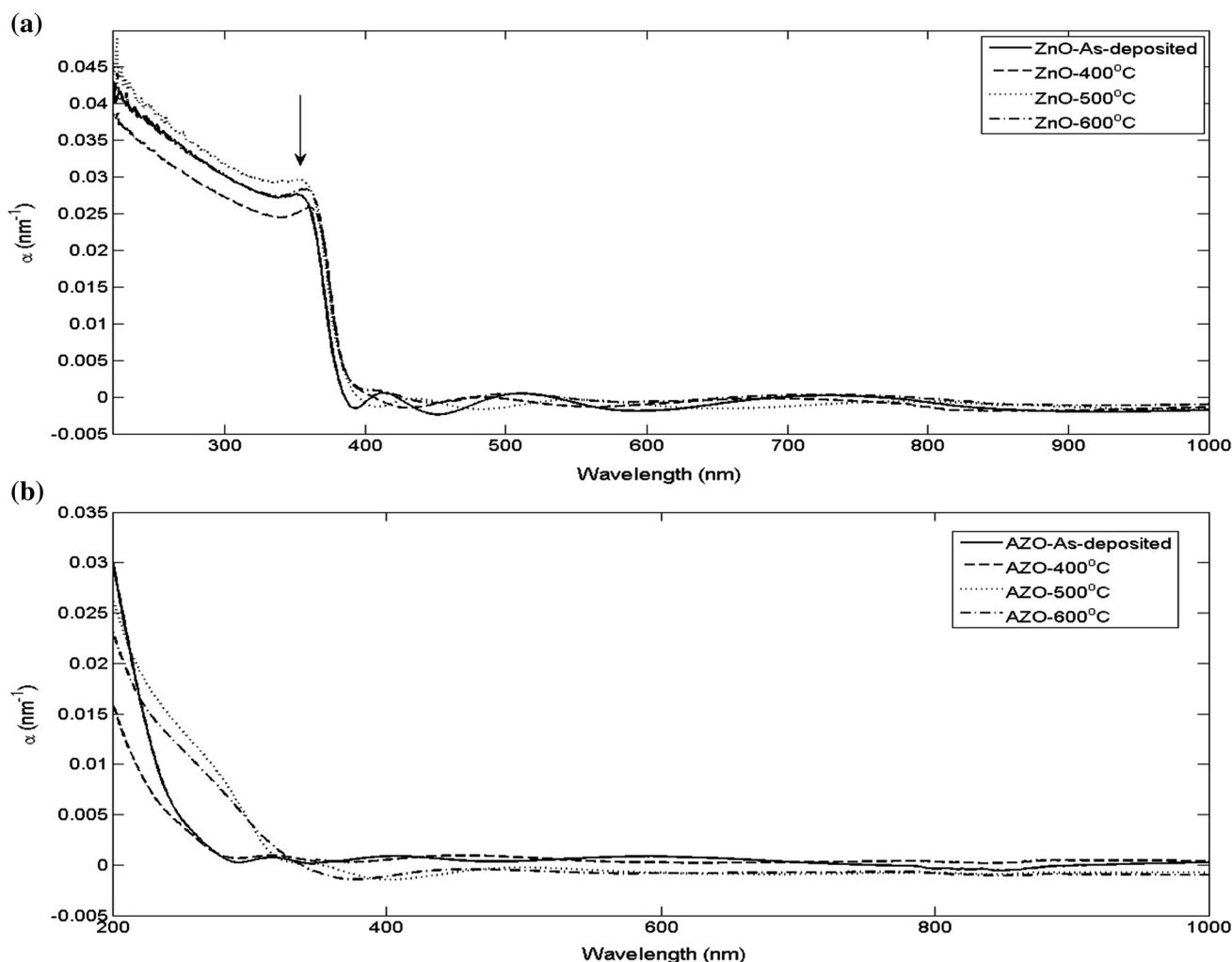


**Fig. 7** Absorption coefficient of **a** ZnO thin films and **b** AZO annealed at different temperatures

since amorphous structure was modified to crystalline and amorphous film band gap was believed to be wider than film with crystalline structure. Generally, AZO films band gaps were wider compared with ZnO films. As annealing temperature increased for both ZnO and AZO films, a reduction of optical band gap was noticed. This could be due to the improvement of crystalline structure. We know that due to the disorder nature of as deposited thin films localized states (traps) are produced in the lowest part of the conduction band and therefore the absorption edge shifts to a higher energy [26, 35]. Hence, larger optical band gap was expected.

Photoluminescence (PL) results of ZnO and AZO films are presented in Figs. 9, 10 and Gaussian fitting was performed for all thin films. It is clear that three different peaks are obtained for as-deposited ZnO film; occurred at 372.34, 407.28, and 441.97 nm which are related to UV, violet, and blue emission, respectively. By annealing ZnO

thin films, UV emission (3.33 eV) and violet emission was found to experience a blue and a red shift, respectively, and a new UV peak was added to the annealed films happened at 391.91 nm. For AZO thin films, four different peaks were procured for as-deposited AZO at 371, 400, and 430 and 453 nm pertained to UV, violet, and blue emission, respectively. However, by annealing at different temperatures, a violet peak was added. The peak at 3.04 eV related to the electron transition from band tail of conduction states to the valance band tail states [35]. On the other hand, this peak due to the annealing produced two new peaks at 3.16 eV (UV emission) and 2.96 eV (violet emission).

The intensity of the violet emission of AZO film annealed at 500 °C increased dramatically in respect to the other film (Fig. 11). Since the optimum conditions for violet emission depend on the crystallinity of the AZO films, so these behaviors could be related to the increase of the grain boundaries as also indicated by AFM study.



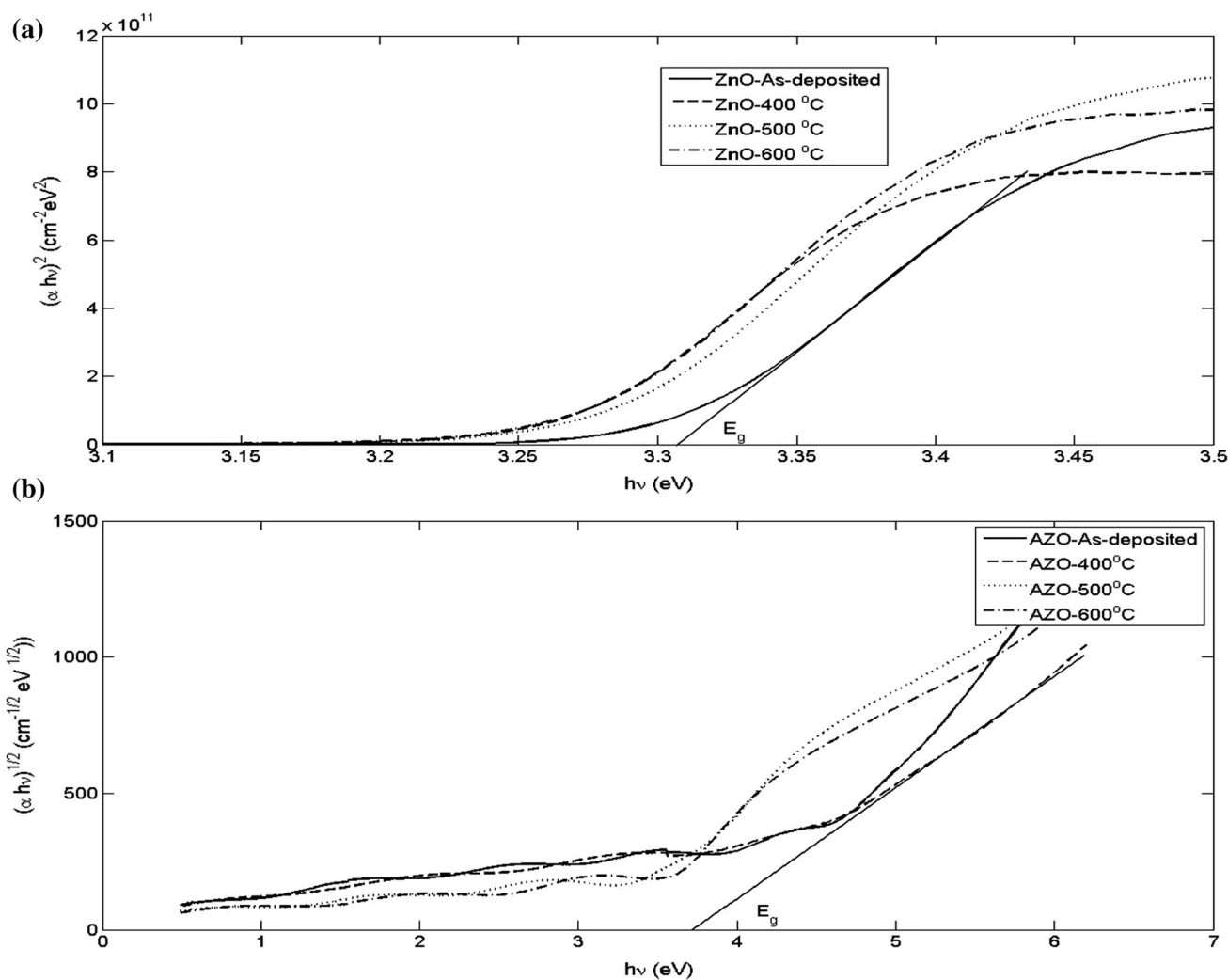


**Fig. 8** a Plot of  $(\alpha hv)^2$  versus Photon energy  $h\nu$  for ZnO films and b Plot of  $(\alpha hv)^{1/2}$  versus Photon energy  $h\nu$  for AZO films at different annealing temperatures

**Table 3** Calculated optical band gap of ZnO and AZO thin films

Sample	$E_g$ (eV)
ZnO	3.31
ZnO-400 °C	3.26
ZnO-500 °C	3.28
ZnO-600 °C	3.26
AZO	4
AZO-400 °C	3.7
AZO-500 °C	3.4
AZO-600 °C	3.4

Hence, it could be concluded that aluminum doping and annealing at 500 °C led to significant increment of violet emission intensity which can be used for light emitting diode and biological fluorescence labeling applications [22].

### 4 Conclusion

We prepared ZnO and AZO thin films by reactive RF magnetron sputtering. The conducted experiment highlighted the influence of both annealing and Al doping of ZnO thin films by argon gas at various annealing temperatures. Comparison of films properties showed that Al doping and annealed at 500 °C improved crystalline structures, grain sizes, and transmittance of the films, dramatically. RMS roughness of both ZnO and AZO films highlighted that all films roughness’s were so small in comparison with films thicknesses which were in the range 6.15–9.42 for ZnO and AZO were in the range 3.50–3.87 nm. Histogram plots showed that for almost all films, crystalline sizes increased by increment of annealing temperature. Optical band gap determination showed that post-annealing resulted in narrowing band gap of

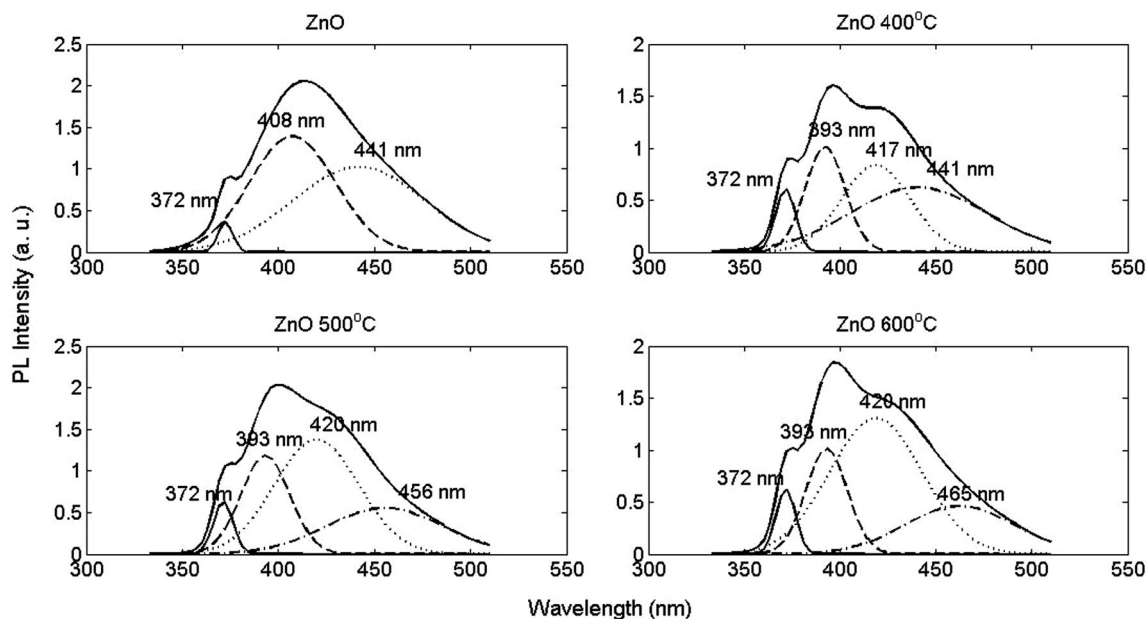


**Fig. 9** Room temperature Photoluminescence spectrum of ZnO films with Gaussian fitting at different temperatures

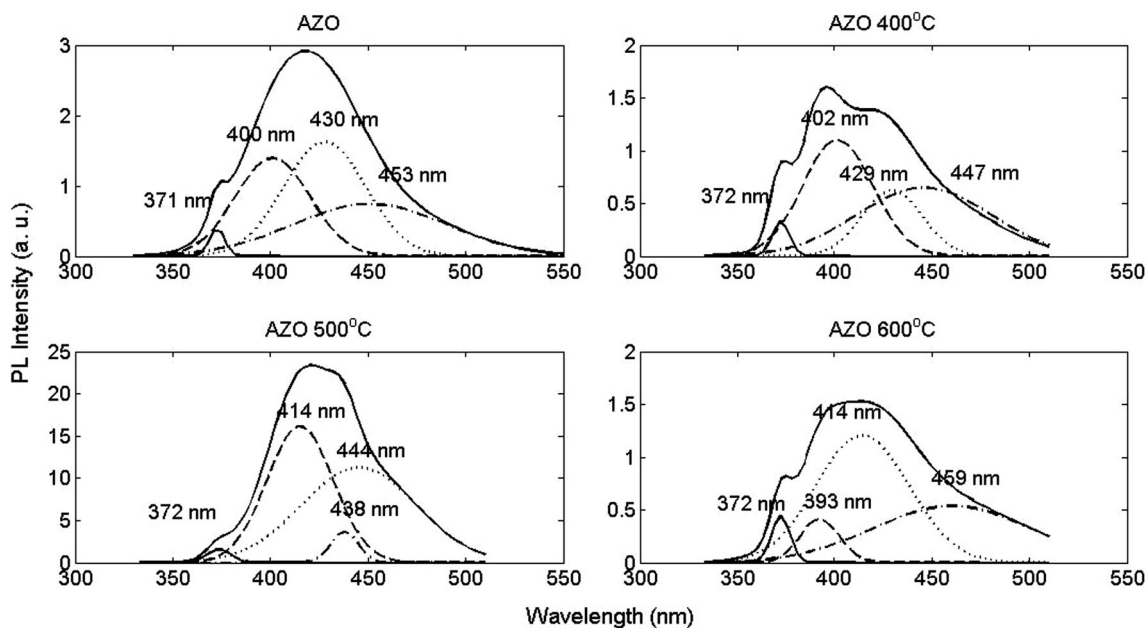


**Fig. 10** Room temperature Photoluminescence spectrum of AZO films with Gaussian fitting at different temperatures

annealed films compared to as-deposited ones. Al doping in ZnO films showed that at the same annealing temperature, optical band gap of AZO films were wider than ZnO films. Al doping introduces some new emission peaks in PL. Moreover, the emission intensities of UV, violet, and blue of AZO annealed films increased and green emission was observed neither in ZnO nor AZO films. Temperature can stimulate the migration of grain

boundaries and cause the coalescence of more grains during annealing processes [36] the grain size measured from AFM is the surface morphology of coalesced grains which gives the particle size. This also agrees with the results shown in XRD which confirms that crystalline size is increased. Also, the enhanced annealing temperature cause decrease in band gap due to quantum confinement [37].

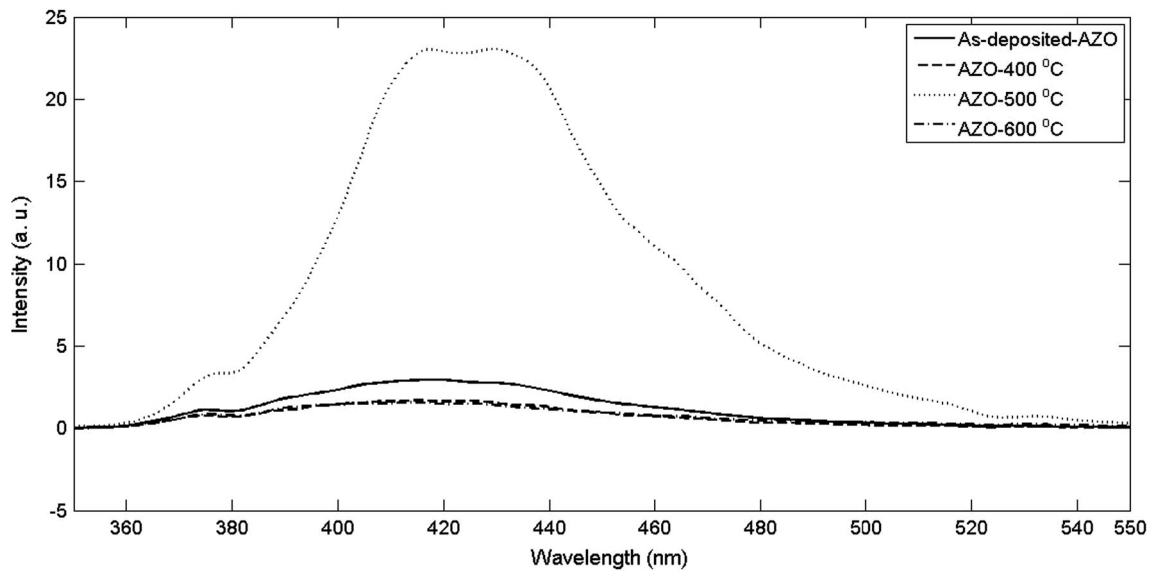


**Fig. 11** PL spectra of AZO thin films annealed at different temperatures

### Compliance with ethical standards

**Conflict of interest** The authors report no conflict of interests. The authors alone are responsible for the content and writing of the paper.

### References

- X.-H. Lu, D. Wang, G.-R. Li, C.-Y. Su, D.-B. Kuang, Y.-X. Tong, Controllable electrochemical synthesis of hierarchical ZnO nanostructures on FTO Glass. *J. Phys. Chem. C* **113**, 13574–13582 (2009)
- L. Zhang, K. Jin, S. Li, L. Wang, Y. Zhang, X. Li, Synthesis of flower-Like ZnO films and their photovoltaic properties for dye-sensitized solar cells. *J. Electr. Mater.* **44**, 244–251 (2015)
- K. Pradhan, R.M. Mundle, K. Santiago, J.R. Skuza, B. Xiao, K.D. Song, M. Bahoura, R. Cheaito, P.E. Hopkins, Extreme tunability in aluminum doped Zinc Oxide plasmonic materials for near-infrared applications. *Sci. Rep.* **4** (2014)
- T. Minami, Y. Nishi, T. Miyata, Effect of the thin Ga2O3 layer in n + -ZnO/n-Ga2O3/p-Cu2O heterojunction solar cells. *Thin Solid Films* **549**, 65–69 (2013)
- H. Masui, S. Nakamura, S.P. DenBaars, U.K. Mishra, Nonpolar and semipolar iii-nitride light-emitting diodes: achievements and challenges. *Electron Devices IEEE Trans.* **57**, 88–100 (2010)
- X. Jiang, F.L. Wong, M.K. Fung, S.T. Lee, Aluminum-doped zinc oxide films as transparent conductive electrode for organic light-emitting devices. *Appl. Phys. Lett.* **83**, 1875–1877 (2003)
- L. Chow, O. Lupan, G. Chai, H. Khallaf, L.K. Ono, B. Roldan Cuenya, I.M. Tiginyanu, V.V. Ursaki, V. Sontea, A. Schulte, Synthesis and characterization of Cu-doped ZnO one-dimensional structures for miniaturized sensor applications with faster response. *Sens. Actuators A* **189**, 399–408 (2013)
- W. Li, J. Chen, H. Cui, F. Liu, X. Hao, Inhibiting MoS2 formation by introducing a ZnO intermediate layer for Cu2ZnSnS4 solar cells. *Mater. Lett.* **130**, 87–90 (2014)
- P. Yang, H. Yan, S. Mao, R. Russo, J. Johnson, R. Saykally, N. Morris, J. Pham, R. He, J.H. Choi, Controlled growth of ZnO nanowires and their optical properties. *Adv. Funct. Mater.* **12**, 323 (2002)
- S. Sadjadi, M. Eskandari, Ultrasonic assisted synthesis of imidazo[1,2-a]azine catalyzed by ZnO nanorods. *Ultrason. Sonochem.* **20**, 640–643 (2013)
- Z. Zang, M. Wen, W. Chen, Y. Zeng, Z. Zu, X. Zeng, X. Tang, Strong yellow emission of ZnO hollow nanospheres fabricated using polystyrene spheres as templates. *Mater. Des.* **84**, 418–421 (2015)
- Z. Zang, X. Tang, Enhanced fluorescence imaging performance of hydrophobic colloidal ZnO nanoparticles by a facile method **619**, 98–101 (2015)
- Y. Sun, D.J. Riley, M.N.R. Ashfold, Mechanism of ZnO nanotube growth by hydrothermal methods on ZnO film-coated Si substrates. *J. Phys. Chem. B* **110**, 15186–15192 (2006)
- S. Țălu, S. Stach, S. Solaymani, R. Moradian, A. Ghaderi, M.R. Hantehzadeh, S.M. Elahi, Z. Garczyk, S. Izadyar, Multifractal spectra of atomic force microscope images of Cu/Fe nanoparticles based films thickness. *J. Electroanal. Chem.* **749**, 31–41 (2015)
- S. Țălu, S. Stach, T. Ghodselahi, S. Solaymani, A. Ghaderi, A. Boochani, Z. Garczyk, Topographic characterization of Cu–Ni NPs @ a-C: H films by AFM and multifractal analysis. *J Phys. Chem. B* **119**(17), 5662–5670 (2015)
- S.T. Tan, B.J. Chen, X.W. Sun, W.J. Fan, H.S. Kwok, X.H. Zhang, S.J. Chua, Blueshift of optical band gap in ZnO thin films grown by metal-organic chemical-vapor deposition. *J. Appl. Phys.* **98** (2005)
- A. Ghaderi, S.M. Elahi, S. Solaymani, M. Naseri, M. Ahmadirad, S. Bahrami, A.E. Khalili, Thickness dependence of the structural and electrical properties of ZnO thermal-evaporated thin films. *PRAMANA J. Phys* **77**(6), 1–8 (2011)
- P. Jin, S. Nakao, S.X. Wang, L.M. Wang, Localized epitaxial growth of  $\alpha$ -Al2O3 thin films on Cr2O3 template by sputter deposition at low substrate temperature. *Appl. Phys. Lett.* **82**, 1024–1026 (2003)
- T.L. Yang, D.H. Zhang, J. Ma, H.L. Ma, Y. Chen, Transparent conducting ZnO: Al films deposited on organic substrates deposited by r.f. magnetron-sputtering. *Thin Solid Films* **326**, 60–62 (1998)
- Y. Lin, J. Xie, H. Wang, Y. Li, C. Chavez, S. Lee, S.R. Foltyn, S.A. Crooker, A.K. Burrell, T.M. McCleskey, Q.X. Jia, Green

- luminescent zinc oxide films prepared by polymer-assisted deposition with rapid thermal process. *Thin Solid Films* **492**, 101–104 (2005)
21. L.B. Duan, X.R. Zhao, J.M. Liu, W.C. Geng, H.Y. Xie, H.N. Sun, Effect of annealing ambient on the structural, optical and electrical properties of (Mg, Al)-codoped ZnO thin films. *Phys. Scr.* **85**, 035709 (2012)
  22. Z. Liang, X. Yu, B. Lei, P. Liu, W. Mai, Novel blue-violet photoluminescence from sputtered ZnO thin films. *J. Alloy. Compd.* **509**, 5437–5440 (2011)
  23. S. Cho, J. Ma, Y. Kim, Y. Sun, G.K.L. Wong, J.B. Ketterson, Photoluminescence and ultraviolet lasing of polycrystalline ZnO thin films prepared by the oxidation of the metallic Zn. *Appl. Phys. Lett.* **75**, 2761–2763 (1999)
  24. H. Chen, H.-J. Jin, C.-B. Park, Influence of hydrogen on Al-doped ZnO thin films in the process of deposition and annealing. *Trans. Electr. Electron. Mater.* **10**, 93–96 (2009)
  25. E.S. Shim, H.S. Kang, S.S. Pang, J.S. Kang, I. Yun, S.Y. Lee, Annealing effect on the structural and optical properties of ZnO thin film on InP. *Mater. Sci. Eng. B* **102**, 366–369 (2003)
  26. F.K. Shan, G.X. Liu, W.J. Lee, B.C. Shin, The role of oxygen vacancies in epitaxial-deposited ZnO thin films. *J. Appl. Phys.* **101**, 053106 (2007)
  27. B.D. Cuility, *Elements of X-ray Diffraction* (Addison-Wesley, Reading, Mass, 1959)
  28. P. Chand, A. Gaur, A. Kumar, Structural, optical and ferroelectric behavior of CuO nanostructures synthesized at different pH values. *Superlattices Microstruct.* **60**, 129–138 (2013)
  29. H. Morkoç, U. Özgür, *Zinc oxide fundamentals, materials and device technology* (Wiley-VCH, Weinheim, 2009)
  30. J.M. Yuk, J.W. Shin, J.Y. Lee, D.I. Son, J.H. Jung, T.W. Kim, J.Y. Kim, W.K. Choi, Effect of thermal annealing on the formation of preferential c-axis orientation and an interfacial layer for ZnO thin films grown on an n-Si (001) substrate. *J. Korean Phys. Soc.* **50**, 4 (2007)
  31. S. Salleh, M.N. Dalimin, H.N. Rutt, Structural and surface characterization of cold deposited zinc sulfide thin films, in *3rd International Conference on Solid State Science and Technology (ICSSST2010)*, Universiti Malaysia Sarawak, 2010
  32. K.-S. Hwang, Y.-J. Lee, S. Hwangbo, Growth, structure and optical properties of amorphous or nano-crystalline ZnO thin films prepared by prefiring-final annealing. *J. Ceram. Process. Res.* **8**, 7 (2007)
  33. M. Fox, *Optical properties of solids* (OUP, Oxford, 2010)
  34. J. Tauc, R. Grigorovici, A. Vancu, Optical properties and electronic structure of amorphous Germanium. *Phys. Status Solidi* **15**, 627–637 (1966)
  35. M.H. Cohen, H. Fritzsche, S.R. Ovshinsky, Simple band model for amorphous semiconducting alloys. *Phys. Rev. Lett.* **22**, 1065–1068 (1969)
  36. Y. Lin, J. Xie, H. Wang, Y. Li, C. Chavez, S. Lee, S.R. Foltyn, S.A. Crooker, A.K. Burrell, T.M. McCleskey, Q.X. Jia, *Thin Solid Films* **101**, 492 (2005)
  37. Sunglae Cho, Jing Ma, Yunki Kim, Yi Sun, G.K.L. George, J.B. Ketterson, *Appl. Phys. Lett.* **75**, 2761 (1999)